arXiv:cond-mat/0207208v1 [cond-mat.stat-mech] 8 Jul 2002

Universal and non-universal properties of transitions to spatio-temporal chaos in coupled map lattices.

René Mikkelsen,[1] Martin van Hecke,[2] and Tomas Bohr[3]

[1] *Center for Chaos and Turbulence Studies, The Niels Bohr Institute, Blegdamsvej 17, DK-2100, Copenhagen Ø, Denmark*

[2] *Kamerlingh Onnes Laboratory, University of Leiden, Niels Bohrweg 2, 2333 CA, Leiden, The Netherlands.*

[3] *Department of Physics, The Danish Technical University, DK-2800 Kgs. Lyngby, Denmark*

(Dated: March 22, 2022)

We study the transition from laminar to chaotic behavior in deterministic chaotic coupled map lattices and in an extension of the stochastic Domany–Kinzel cellular automaton [1]. For the deterministic coupled map lattices we find evidence that "solitons" can change the *nature* of the transition: for short soliton lifetimes it is of second order, while for longer but *finite* lifetimes, it is more reminiscent of a first order transition. In the second order regime the deterministic model behaves like Directed Percolation with infinitely many absorbing states; we present evidence obtained from the study of bulk properties and the spreading of chaotic seeds in a laminar background. To study the influence of the solitons more specifically, we introduce a soliton including variant of the stochastic Domany–Kinzel cellular automaton. Similar to the deterministic model, we find a transition from second to first order behavior due to the solitons, both in a mean field analysis and in a numerical study of the statistical properties of this stochastic model. Our study illustrates that under the appropriate mapping some deterministic chaotic systems behave like stochastic models; but it is hard to know precisely which degrees of freedom need to be included in such description.

PACS numbers: 05.45.+b, 05.70.Jk, 47.27.Cn

I. INTRODUCTION.

Spatiotemporal chaos (STC) occurs in many spatially extended deterministic systems and remains notoriously difficult to characterize [2]. Therefore one may attempt to map such deterministic chaotic systems onto stochastic models for which many more analytical methods are available. It is then tacitly assumed that, after sufficient coarse graining of the deterministic model, the role of deterministic chaos can be taken over by the noise in the stochastic system. A critical test of the validity of such mappings are the predictions for the transitions between qualitatively different states that extended chaotic systems display. The key question is then: *are transitions in deterministic chaotic systems governed by the universality classes of stochastic systems?*

As is known for a variety of spatiotemporal chaotic systems [2, 3] and as we will show below for the deterministic system at hand, chaotic states in extended systems often display a mixture of rather regularly propagating structures and more disordered behavior. When the propagating structures, that we will refer to as "solitons" (following [4]) have a finite lifetime, it may seem that they can be ignored after sufficient coarse graining. We will find strong indications that this is *not* always the case, and we will give an example where their influence may even be so strong as to change the nature of the transition. We will also show that extending simple stochastic models with the appropriate solitonic degrees of freedom can mimic this behavior quite accurately: not only can we change the order of the transition, we can also get transient non-universal scaling of the type observed in coupled map lattices [5]. Therefore we conclude that, in many cases, deterministic chaotic systems *can indeed* be mapped to stochastic models. A short account of our work has already been published [6].

A. Historical background

Chaté and Manneville [7] introduced the notion of a universal transition to extended chaos via "spatiotemporal intermittency" (STI) [8, 9] in a study of the *deterministic* damped Kuramoto-Sivashinsky partial differential equation [10]. STI states are composed of "turbulent" (chaotic) and "laminar" (ordered) patches, and the laminar patches remain so except for contamination by turbulence at their boundaries. These states are conjectured to occur quite generally when, locally, laminar and turbulent dynamics are separated by a subcritical bifurcation, and indeed a large number of different experimental systems and theoretical models display STI [9].

As a function of their parameters, STI systems display a transition from states where the turbulence eventually dies out to states where the turbulence spreads and dominates. Pomeau proposed [11] an analogy between this transition and the phase transition of the stochastic process known as Directed Percolation (DP); for an introduction to DP, see e.g. [12, 13]. In directed percolation one considers the spreading of "activity" in an absorbing, inactive background. Earlier, Grassberger [14] and Janssen [15] had conjectured that any *stochastic* process with an unique absorbing state should be in the same di-

rected percolation universality class.

Relating laminar to inactive and turbulent to active states appears to map spatiotemporal intermittency to directed percolation. To verify whether *deterministic* chaotic models with an absorbing state would be in the DP universality class, Chaté and Manneville introduced a very simple coupled map lattice (CML) that displays STI and numerically obtained the critical exponents that characterize the transition from inactive to active states. Surprisingly, these critical exponents appear to vary with the parameters and are in general different from the DP values. Therefore the Chaté–Manneville model appears to be *not* in the DP universality class and not even universal.

Grassberger and Schreiber [4] pointed out that the presence of long lived traveling structures which they call "solitons" in the Chaté–Manneville model may lead to large crossover times, and conjectured that in the long-time limit the behavior of the Chaté–Manneville model would be in the DP universality class.

Recently, the Chaté–Manneville model with an asynchronous update rule was studied [16]. Here random sites are chosen to be iterated forward while keeping the others unaltered. For this model, the solitons observed for the standard synchronous update rule are suppressed and the critical exponents are universal with DP values, implying that the Chaté–Manneville model with asynchronous updating belongs to the DP universality class. However, the asynchronous updating introduces an element of stochasticity into the model, thus ruining the deterministic character of the original model.

B. Outline

In this paper we will study a *deterministic* extension of the Chaté–Manneville CML that facilitates the tuning of the soliton properties. We will demonstrate that the influence of solitons may be much more profound than setting a crossover time, since they appear to be able to change the type of transition from second to first order. The role of the solitons is further illustrated in an extension of the *stochastic* Domany-Kinzel cellular automaton. In its standard form, all sites of this model can be either active or inactive, but we will add a "solitonic" degree of freedom that mimics the behavior of the solitons in the CML's. The mean field equations of this stochastic model show a transition from second order DP-like, behavior to a first order transition when the soliton lifetimes are increased. Numerical studies of this stochastic model also find evidence for such a crossover to first order behavior, although it is very difficult to asses the asymptotic behavior for our model. In any case, we present strong numerical evidence that the transition is not an ordinary second order transition and that there is no asymptotic scaling regime, although there are appears to be a transient which displays non-universal scaling behavior.

Our study illustrates that for extended systems it is a difficult task to faithfully map a deterministic system to a stochastic counterpart. In this particular case, localized propagating structures can be identified as responsible for the breakdown of DP universality, but one can imagine that less easily identified properties of the deterministic dynamics could be responsible for such a breakdown in other systems.

The outline of this paper is as follows. In section II we discuss the coupled map lattices. Starting from a brief discussion of the classic Chaté-Manneville model, we introduce our extension to lattices of two-dimensional maps in section II A. We show that the new parameter that is introduced has a profound effect on the importance of "solitons", and that long living solitons change the transition from inactive to active states from a second to a first order transition in section II B. In the second order regime, we estimate the bulk critical exponents using finite size scaling techniques in section II C, and measure spreading exponents in section II D. All this data is consistent with the coupled map lattice being in the universality class of Directed Percolation with infinitely many absorbing states, provided that soliton lifetimes are short. In section III we discuss the extension of the standard Domany-Kinzel cellular automata which includes new degrees of freedom that mimic the solitons of the coupled map lattices. The mean field equations for this model are studied in section III B, and these show a transition from second to first order behavior as a function of the soliton lifetimes. We study the phenomenology and its statistical bulk properties of the full model in the soliton rich regime in section III C. The behavior of the model in the soliton rich regime is quite distinct from an ordinary second order transition.

II. COUPLED MAP LATTICES.

The model introduced by Chaté and Manneville consists of coupled maps, each of which either performs "laminar" or chaotic motion. The model was motivated by the fact that studies of the deterministic partial differential equations, such as the damped Kuramoto-Sivashinsky equation, are numerically quite demanding and had not provided enough precision to allow a definitive comparison to DP [5, 7]. In one spatial dimension their coupled map lattice was defined according to

$$u_i(n+1) = f(u_i(n)) + \frac{\varepsilon}{2}\Delta_f u_i(n) \qquad (1)$$

where the subscripts i denote the spatial position, n is the discrete time and $\Delta_f u_i(n) = f(u_{i-1}(n)) - 2f(u_i(n)) + f(u_{i+1}(n))$. This expression is a discrete approximation of diffusive coupling in one dimension and introduces spatial correlations in the system; the parameter ε is a measure of the coupling strength between a site i and its two nearest neighbors at sites $(i-1)$ and $(i+1)$.

The map f is chosen such that locally the scalar field u_i can be in either of two states: the absorbing (laminar) or

the chaotic (turbulent) one. When $u < 1$, f is a standard tent map of the form $f(u) = r(\frac{1}{2} - |u - \frac{1}{2}|)$ which displays chaotic behavior, while in the region where $u > 1$, f is simply the identity and leads to a laminar state. The sharp discontinuity in f ensures that the two states are distinguishable at each site. The parameter $r > 2$ determines the steepness of the tent map as well as the transition ratio from the chaotic to the laminar regime in the absence of coupling.

The form of the diffusive coupling ensures that turbulent sites cannot be spontaneously generated in a background of laminar sites: states where all sites are laminar remain so, and the laminar state is truly absorbing. The laminar state is not unique: Updating a state where all sites are in the laminar regime ($u_i > 1$) leads, via the diffusion operator, to a state where all variables are equal to the global average value $\bar{u}$.

Once initiated, turbulent activity can spread through this CML by infecting laminar patches from their boundaries. The effectiveness of the resulting spreading of the chaos depends on the values of r and ε. Suppose we study the behavior of this system by keeping r fixed while varying the coupling strength ε. Completely analogous to DP, a critical value $\varepsilon = \varepsilon_c(r)$ exists, such that for $\varepsilon < \varepsilon_c$ an absorbing state is reached with unit probability while sustained chaotic behavior (in the thermodynamic limit) is found for $\varepsilon > \varepsilon_c$. Taking the density of chaotic sites or "activity" m as an order parameter, transitions from a "laminar" state (where m decays to zero) to a "turbulent" state (where m reaches a finite value in an infinite system) can be studied.

A. Extensions to two-dimensional maps

Coupled map lattice's can, in principle, be related to continuous time physical systems of weakly coupled elements by interpreting the map f as a return map on a Poincaré section. The time spent by two different sites between successive returns would in general be different for systems without periodic external forcing, and this was precisely the motivation for the asynchronous update rule in [16]. However, here we wish to mimic the variations in return times in a *deterministic* fashion. This motivated us to introduce a second field in the CML. Note that the simplest chaotic oscillator would be a system of three phase space dimensions, like the Lorenz equations. Applying a Poincaré section reduces such a system to a two-dimensional map. This is also the case in systems with external periodic forcing. Here the simplest realization would be systems like a damped nonlinear pendulum or Duffing oscillator with a time-periodic forcing. A Poincaré section again reduces the system to a two-dimensional map and after the synchronous iteration the respective units are still at equal time.

We therefore replace the single variable map $f(u)$ used in Eq. (1), by a new map with an additional variable v:

$$u_i(n+1) = f(u_i(n) + \frac{\varepsilon}{2}\Delta_f u_i(n) + v_i(n) \ , \quad (2)$$

$$v_i(n+1) = b(u_i(n+1) - u_i(n)) \ . \quad (3)$$

Here f is the same map as before and the new parameter b is the Jacobian of the full two-dimensional local map; this map is invertible for any non-zero b and becomes increasingly two-dimensional with $|b|$. The change in the local map (1) is analogous to how the 2D Hénon map [17] is constructed from the 1D logistic map, except that $b(u_i(n+1) - u_i(n))$ appears here on the right hand side instead of $bu_i(n)$. This ensures that the absorbing state fixed points $u_i(n) = u^*$ of the old CML (1) are mapped to the laminar fixed point $(u_i(n), v_i(n)) = (u^*, 0)$ in the new CML. The model (2-3) is a completely deterministic system with no element of stochasticity and is updated synchronously. The value of u_i determines, as in model (1), whether a given site is "active" or "inactive". Starting from the Chaté-Manneville case ($b = 0$) we can follow the transition between laminar and chaotic states. As we will see below, the new parameter b actually opens up the possibility to study the effect of the "solitons" on the dynamical states and transitions of CMLs; this appears to be a more important issue than the dimensionality of the local map.

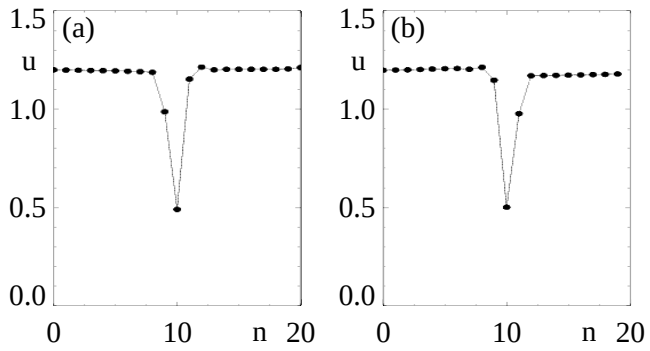


FIG. 1: Average profiles of a right (a) and left (b) moving soliton that occurs in the Chaté-Manneville model at criticality for $r = 3$.

B. Qualitative properties.

Our CML now contains three freely adjustable parameters (r, ε and b), and clearly we will have to focus on a subset of parameters. Our main focus will be on the case where $r = 3$, although we will also study the transition for $r = 2.2$. For $r = 3$ and $b = 0$ the dynamics shows many solitons (see Fig. 1) and the critical exponents appear to differ significantly from those of DP.

To get a feeling for the location of the transition as function of b and ε, we show in figure 2 the activity (defined as the average number of active sites) after 1000 iterations in the ranges $-0.3 \leq b \leq 0.3$ and $0 \leq \varepsilon \leq 0.4$

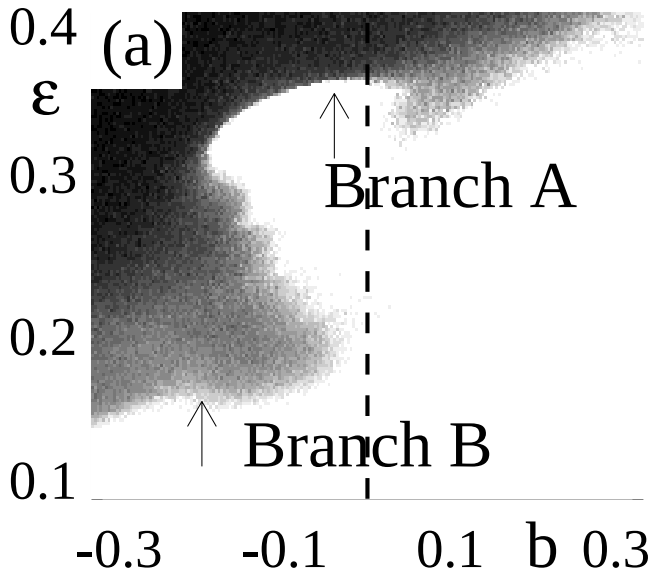


FIG. 2: Activity in the model (2)-(3) at $t = 1000$. White regions correspond to points in the (ε, b)-plane where the initial activity has decayed into an absorbing configuration and the darker regions to points with a non-vanishing order parameter. Clearly the transition curve becomes quite complicated; the two branches discussed in this paper are indicated as "Branch A" and "Branch B" (see text). The dashed line indicates the Chaté-Manneville model ($b=0$)

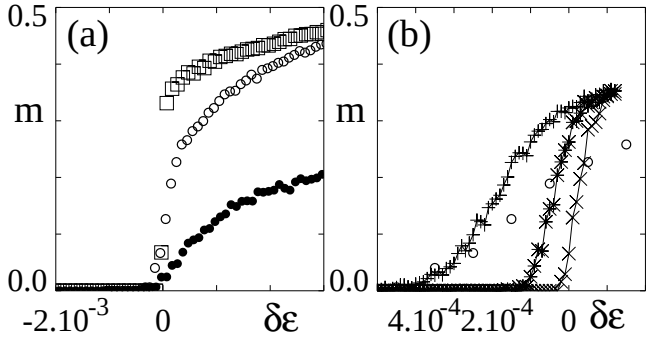


FIG. 3: Activity in the model (2-3) for 128 systems of size $L = 2048$ and $r = 3$. (a) Activity as a function of $\delta\varepsilon$ (distance to the critical point) at time 2×10^5 for $b = -0.1$ (squares), $b = 0$ (open circles) and $b = 0.2$ (closed circles). The transition appears much sharper for negative values of b. (b) Steepening for the transition at $b = -0.1$ for increasing times: 5×10^3 (+), 5×10^4 (*), 5×10^5 (×). To stress the magnified scale of $\delta\varepsilon$, also the data shown in panel (a) for $b = 0$ is plotted (open circles).

at $r=3.0$. The "traditional" transition is that occurring at $b=0$ and $\varepsilon = 0.35984\ldots$. Clearly, for negative values of b two additional transitions emerge. Here we only study points on the two transition branches labeled "A" and "B" in Fig. 2; below we focus on the behavior along branch A.

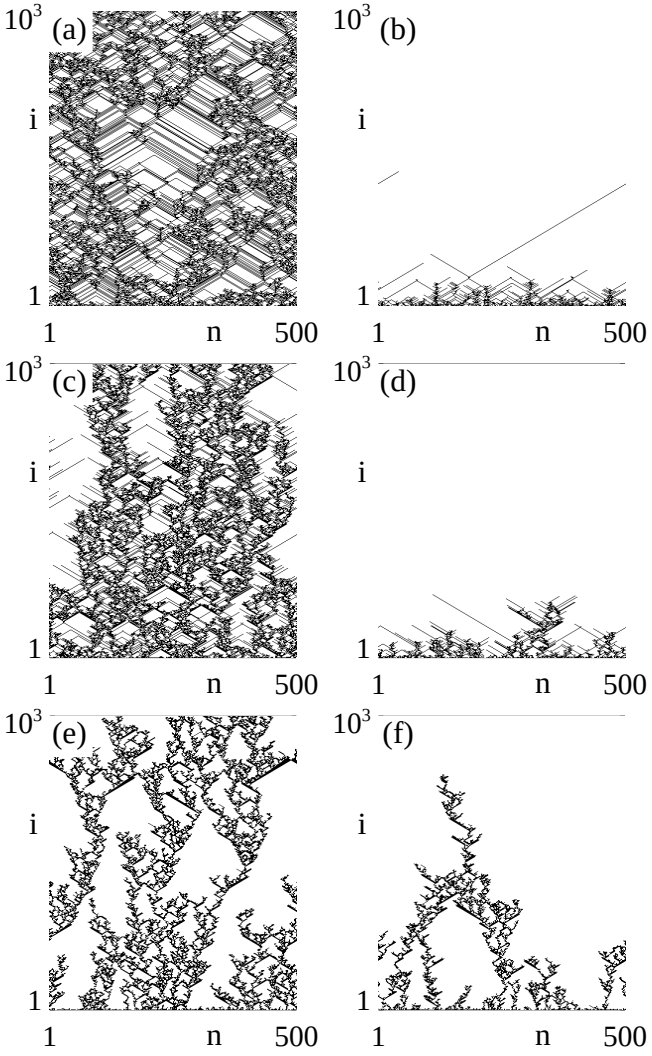


FIG. 4: Spacetime plots of our coupled map lattice (2) -(3) for $r=3$ above (left column) and below (right column) criticality. Inactive sites are white, chaotic sites are black. (a) $b = -0.1$, $\varepsilon = 0.353$ (b) $b = -0.1$, $\varepsilon = 0.343$ (c) $b = 0$ $\varepsilon = 0.361$ (d) $b = 0$, $\varepsilon = 0.351$ (e) $b = 0.2$, $\varepsilon = 0.374$ (f) $b = 0.2$, $\varepsilon = 0.364$.

1. *Qualitative changes in behavior along branch A*

Figure 2 hints that the sharpness of the transition varies along branch A: the jump in order parameter appears to become steeper for negative values of b. The differences in the nature of the transitions are illustrated more clearly in Fig. 3 by plotting the value of the order parameter as a function of ε for $b = 0$ and $b = -0.1$ averaged over an ensemble of 32 systems for a number of times. The behavior for $b = 0$ is consistent with a continuous transition, whereas for $b = -0.1$ longer times lead to a marked steepening, consistent with the emergence of a discontinuity.

a. Soliton regime Some effects of the parameter b on the dynamics can also be seen from the evolution of the binary patterns at $r = 3$ (Fig. 4). For $b = 0$, solitons

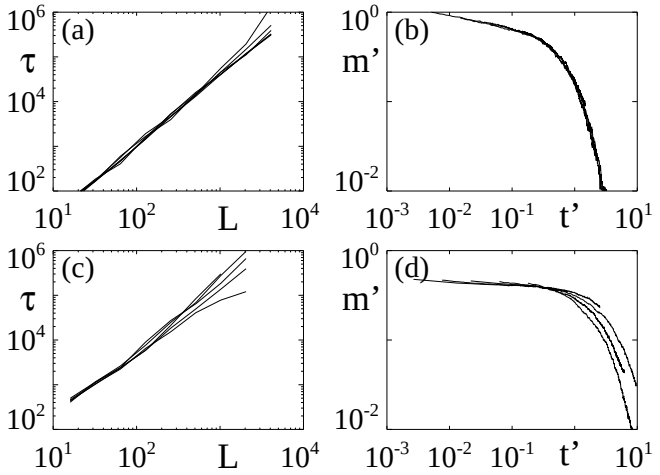


FIG. 5: Examples of good rescaling plots for $b = 0.2$ (a,b) and poor rescaling for $b = -0.1$ (c,d). (a) Absorption time τ vs. systemsize L, for $r = 3, b = 0.2$ and $\varepsilon = 0.3727, 0.37322, 0.37323$ (critical value), $0.37325, 0.3733$ and 0.3735. (b) Rescaled average activity $m' := mL^{-\theta}$ versus rescaled time $t' := t/L^z$ for $r = 3, b = 0.2$ and $\varepsilon = 0.37323$ for $L = 32, 64, 128, 256$ and 512, showing a good data collapse. (c) Absorption time τ vs. systemsize L, for $r = 3, b = -0.1$ and $\varepsilon = 0.35200, 0.35203, 0.35205, 0.35206$ and 0.35207. Even small changes in ε lead to substantial changes in the absorption time, and it is difficult to estimate the critical value of ε. (d) Rescaled average activity m' versus rescaled time t' for $r = 3, b = -0.1$ and $\varepsilon = 0.35203$ for $L = 64, 128, 256, 512$ and 1024, showing poor data collapse; either the initial decay or the tails do not overlap; shown here is a compromise. Note that the initial decay is very slow, leading to a small estimate for the value of θ.

can be seen both above and below threshold (Fig. 4c-d). They consist of pairs of active sites and propagate with velocity one. Their maximal lifetimes are of order 100 (Fig. 4d). When b is decreased to a value of -0.1, the typical lifetimes of solitons become so long that they typically only vanish when they collide with other solitons or propagate into turbulent structures. When two solitons collide, they either annihilate or create new turbulent structures. Such creation is clearly visible in Fig. 4a for $n \approx 200$ and $i \approx 600$.

For sufficiently large b the isolated solitons present in the original model ($b = 0$) are suppressed: solitons with a lifetime longer than a few iterations are rare here. On the other hand, there are regular "edge" states visible, where an active state propagates ballistically while emitting new activity; one example is visible in Fig. 4e for $n \approx 400$ and $i \approx 800$. These structures do not seem to influence the order of the transition, but they may very well lead to rather large crossover scales.

In conclusion: the value of b has a large influence on the presence of solitons, and also influences the steepness of the transition. In fact; discontinuities are found at points in (ε, b)-space where solitons dominate the dynamics. This implies that the (colliding) solitons have a strong influence on the global dynamics and are able to change the nature of the transition from a continuous to what appears as a first order one. We will make this point more precise below.

C. Finite size scaling in 2nd order regime

Stochastic systems belonging to the DP universality class are characterized by a set of critical exponents describing, e.g., the order parameter $m(\varepsilon, L, t)$ and the behavior of the "absorption time" $\tau(r, \varepsilon, L)$, i. e. the averaged time it takes the system, starting from a random initial state, to reach the absorbing state. From finite-size scaling arguments [18], one finds that the order parameter m at the critical point ε_c should behave as

$$m(L, t) \sim L^{-\beta/\nu_\perp} g(t/L^z) \ . \tag{4}$$

For a finite lattice, the absorption time τ then increases as

$$\tau \sim L^z \ . \tag{5}$$

Finally, for short times ($t \ll L^z$), $g(t/L^z) \sim (t/L^z)^{-\beta/\nu_\parallel}$, so that for short times m should decay as

$$m(L, t) \sim t^\theta \quad for \quad t << L^z \tag{6}$$

Here the usual dynamical exponent $z = \nu_\parallel/\nu_\perp$ has been introduced, defined as the ratio between the correlation length exponent in the time direction $\nu_\parallel$ and the correlation length exponent in space $\nu_\perp$. The scaling relation $\theta = -\beta/\nu_\parallel$ connects the critical exponents.

To estimate the critical exponents for our CML we performed direct numerical simulations and calculated the absorption time τ and the order parameter m, defined as the average activity. We used ensembles of initial conditions, in which all initial u values are assigned a random value in the chaotic phase, $0 \le u_i(0) \le 1$. The v-values of the initial state are set to zero to ensure that they do not influence the u-values from the onset of iteration and that the analogy with the original model and our variant at $b = 0$ is satisfied.

The behavior of the absorption time at criticality is used to determine the critical point and the z exponent [16, 18]. An ensemble of 128 systems is iterated forward in time until an absorbing configuration is reached. The average number of time steps needed before reaching such a configuration yields the absorption time τ. Examples of τ as function of L are shown in Fig. 5a,c; the best fit to a straight slope determines the critical exponent z.

In Fig. 5b,d we plot examples of $m' := mL^{-\theta}$ as function of $t' := t/L^z$ for a range of L's. When proper scaling occurs, as is the case in Fig. 5b, the curves for different L fall on top of each-other, and the initial power-law decay of m' determines the exponent θ. Here an ensemble of 1000 systems was used. The order parameter was calculated as the sum of active sites divided by the total amount of sites. The systems are iterated forward until $t \approx L^z$, where the algebraic behavior clearly ends.

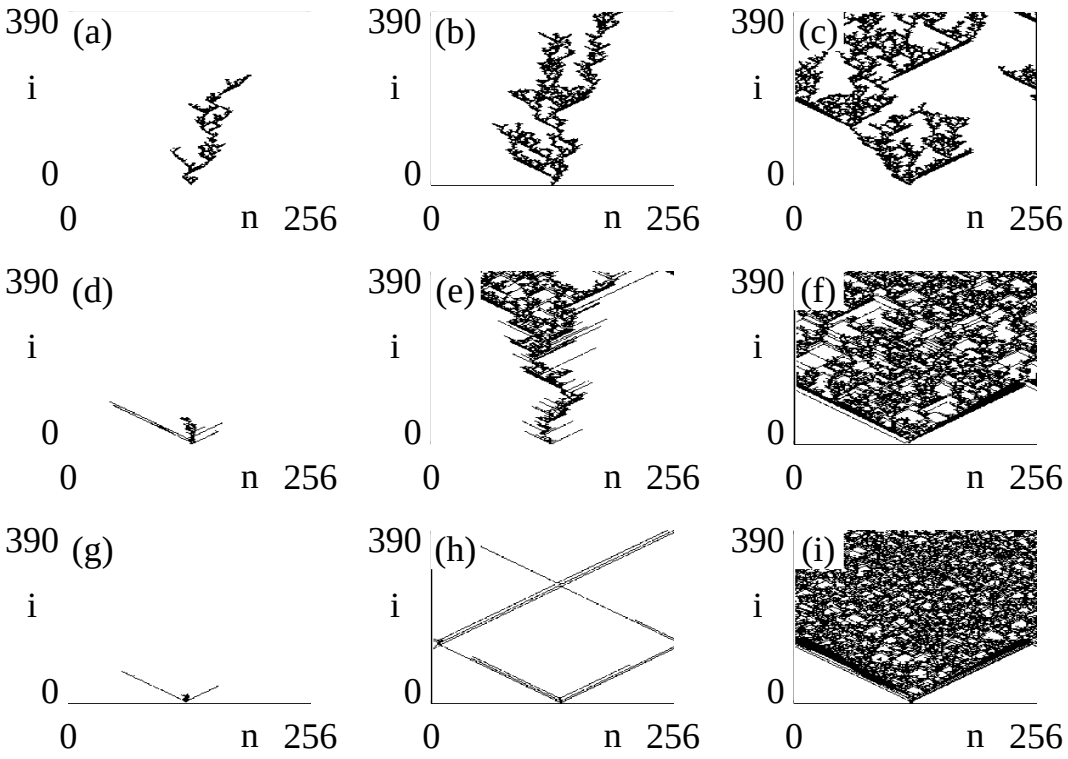


FIG. 6: Spreading of a single turbulent seed through the "natural-initial-state" below criticality, at criticality and above criticality, for $b = 0.2$ (a-c), the Chaté–Manneville model for $b=0$ (d-f) and $b = -0.1$ (g-i). In all cases $r = 3.0$.

Estimates of critical exponents have been done for $r = 2.2$ and $r = 3.0$. For $r = 3.0$, the critical exponents for the original model ($b = 0$) shows significant deviations from the corresponding DP values and the computational costs are tolerable. In Fig. 5a,b we show examples of the rescaling plots for $r = 3, b = 0.2$, where a nice data-collapse occurs and the transition appears to be of 2nd order, and for $r = 3, b = -0.1$ (Fig. 5c,d), where the data-collapse is poor and the transition appears to be no longer continuous.

The values of the critical exponents are given in Table I and correspond simply to the best possible values, irrespective of the quality of the data collapse. For $r = 2.2$ DP values are found for $|b| \geq 0.01$. For $r = 3$, the critical transition on Branch B appear to be DP-like, while on Branch A a crossover to DP values is found when b is large enough ($|b| > 0.15$). This regime coincides with values of b where the solitons are suppressed in the space-time plots, and a continuous transition takes place. The soliton dominated dynamics at $b = -0.1$ is reflected in the extremely low value of the exponent θ, characterizing the decay of the order parameter. Here the data-collapse is rather poor as shown in Fig. 5c,d.

D. Spreading of Turbulence in 2nd order regime.

So far the critical properties of the CML's starting from "homogeneous" states have been studied, i.e., with initial conditions where each site in the lattice is assigned a random number in the chaotic (turbulent) phase. A different approach is to consider the spreading of a single turbulent seed in an otherwise laminar configuration (see Fig. 6). This makes it possible to study the dynamical critical exponents, or spreading exponents, and see how these compare to the directed percolation counterparts.

For spreading of activity in stochastic systems with absorbing states the following quantities are characterized by critical exponents [20]: the total number of chaotic sites $N(t)$, the survival probability $P(t)$, the mean-squared deviation $R^2(t)$ of the turbulent activity from the "seed" and the density $n(t)$ of chaotic sites within the spreading patch of turbulence. It is assumed that they behave according to

$$N(t) \sim t^{\eta_s} \quad P(t) \sim t^{-\delta} \quad R^2(t) \sim t^{z_s} \quad n(t) \sim t^{-\theta_s} \qquad (7)$$

For probabilistic systems it has been conjectured and verified numerically [21, 22], that the dynamical exponents satisfy the generalized hyper-scaling relation $\eta_s + \delta + \theta_s = dz_s/2$ where d is the spatial dimension. For systems with

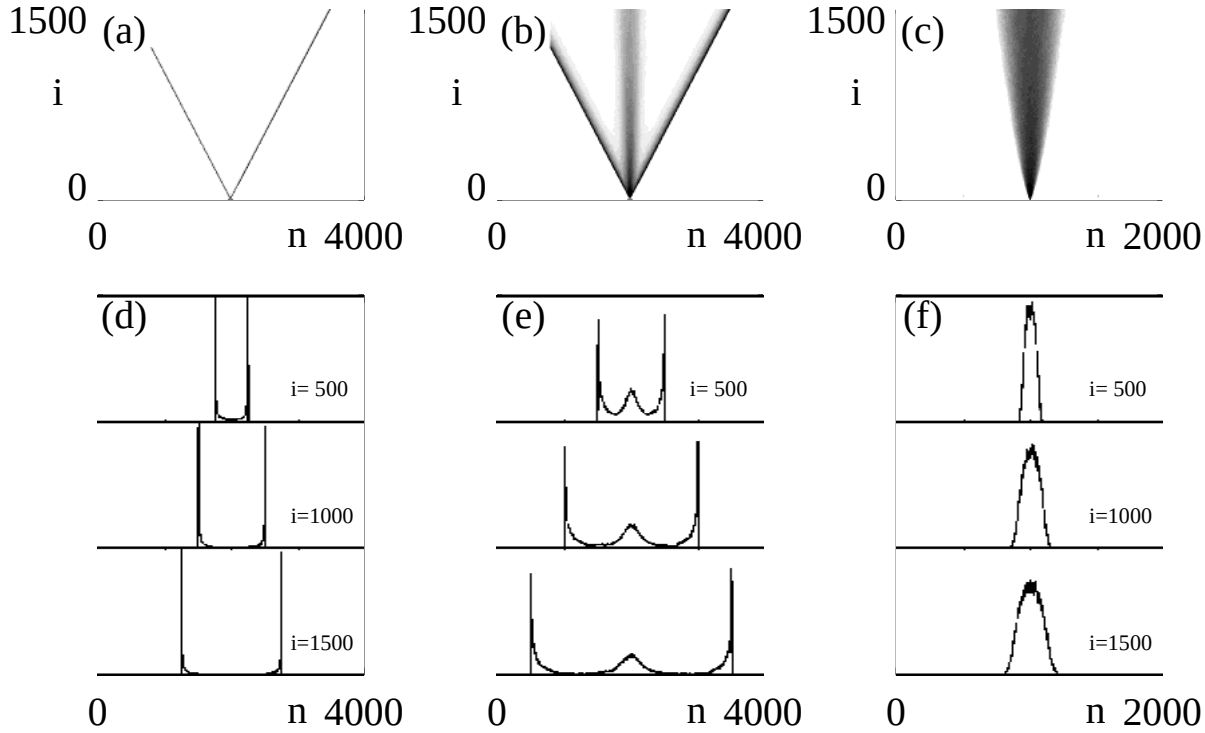


FIG. 7: The average spreading of active seeds in the "natural-initial-state" close to criticality. The densities are obtained by averaging over 10^4 realizations, and for clarity we have included three snapshots of this average activity in the bottom rows of this figure. Parameters are $r = 3$ (for all runs), and $b = -0.1$ (a,d), $b = 0.0$ (b,e) and $b = 0.2$ (c,f). The respective values of natural-initial-state are 1.170, 1.212 and 1.235.

a single absorbing state, including DP, one finds that $\delta = \theta_s = \beta/\nu_{\|}$ and $z_s = 2/z$, reducing the hyper-scaling relation to $4\delta + 2\eta_s = dz_s$.

Systems with infinite numbers of absorbing states have been studied carefully recently and it has been found that they differ from the classical ones (with a single absorbing state belonging to the DP universality class) precisely in the non-universality of the spreading exponents [22]. Only exponents characterizing quantities averaged over surviving runs alone are found to be universal. This implies that z_s, the sum $\eta_s + \delta$ and θ_s are expected to be universal, while η_s and δ individually are not. Only for the so called "natural-initial-state" are the DP values found for the exponents characterizing quantities averaged over all runs. Such a particular state is constructed by letting the system evolve at criticality from homogeneous initial conditions, where all sites initially are in the active phase, until an absorbing configuration is reached.

After a few spreading experiments in our CML we indeed observed that the propagation of activity from the initial seed through the laminar region depended strongly on the configuration of the laminar state surrounding the seed. Moreover the dynamical exponents varied with this configuration, thus being non-universal. So the non-unique absorbing state of our CML (any configuration with all u-values above unity and v-values not too large will be absorbing) leads to behavior as can be expected for DP with an infinite numbers of absorbing states.

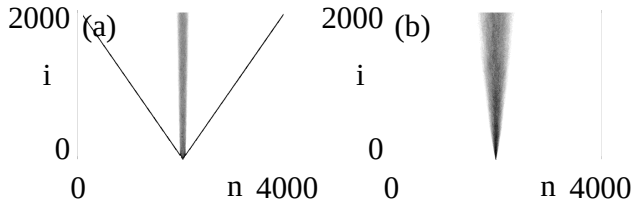


FIG. 8: Average spreading activities near criticality for $r = 3, b = 0.2$ (a) and $r = 3, b = 0$ (b). In comparison to the spreading into the "natural-initial state" as shown in Fig. 6, the value of u in the laminar background has been lowered from 1.235 to 1.225 in (a), thus strongly enhancing solitons, and has been increased from 1.212 to 1.22 in (b), thus strongly suppressing soliton activity.

We determined the "natural-initial-state" by iterating systems of up to 4096 sites from homogeneous initial conditions until an absorbing configuration is reached. The average value of all sites is then used as the value of the laminar background. For $r = 3.0$ we have calculated these as 1.235 for $b = 0.2$, 1.212 for $b = 0$, 1.170 for $b = -0.1$ and 1.0395 for $b = -0.2$.

In Fig. 7 we display the average spreading for $r = 3$ and $b = -0.1, 0$ and 0.2. Clearly, for $b = -0.1$ and for the Chaté–Manneville model at $r = 3, b = 0$ it is basically impossible to estimate the spreading exponents at the "natural-initial-state", since the spreading is dominated

r	b	ε_c	z	θ
2.2	-0.02	0.01338()	1.57(1)	0.16(1)
	-0.01	0.01465()	1.57(1)	0.16(1)
	0.0	0.01605(2)	1.53(1)	0.17(1)
	0.01	0.017628(5)	1.57(1)	0.16(1)
	0.02	0.01921(2)	1.57(2)	0.17(2)
3.0	-0.25	0.16312(3)	1.58(1)	0.160(5)
	-0.2	0.16495(2)	1.58(2)	0.168(3)
	-0.15	0.16205(1)	1.58(1)	0.17(1)
	-0.125	0.16368(2)	1.57(1)	0.20(1)
	-0.1	0.35203(1)	1.52(3)	0.02(2)
	0.0	0.35984(3)	1.42(2)	0.18(1)
	0.1	0.3393(1)	1.48(2)	0.155(1)
	0.125	0.34745(5)	1.53(2)	0.15(1)
	0.15	0.35680(5)	1.57(1)	0.159(3)
	0.175	0.36545(1)	1.58(1)	0.16(1)
	0.2	0.37323(1)	1.58(1)	0.16(1)
DP			1.58074	0.15947

TABLE I: The critical exponents z and $\theta = \beta/\nu_\parallel$ for our CML. The values for DP are taken from [19].

b	x_i	z_s	δ	η_s	θ_s	Δ
0.2	1.229	1.98(2)	0.00(0)			
	1.23	1.68(2)	0.10(1)	0.43(2)	0.32(1)	-0.01(2)
	1.235	1.60(1)	0.16(1)	0.34(1)	0.29(1)	0.01(1)
	1.24	1.61(2)	0.23(2)	0.25(1)	0.31(1)	0.01(2)
	1.245	1.65(1)	0.30(1)	0.23(1)	0.29(2)	0.00(1)
	1.25	1.65(3)	0.34(2)	0.14(1)	0.300(3)	0.05(2)
	1.255	1.69(2)	0.35(2)	0.14(2)	0.29(1)	0.07(2)
	1.26	1.72(3)	0.43(1)	0.04(1)	0.29(1)	0.10(2)
-0.2	1.13	1.99(1)	0.00(0)	0.793(2)	0.205(1)	0.00(1)
	1.135	1.59(2)	0.09(1)	0.42(1)	0.29(1)	-0.01(1)
	1.139	1.58(2)	0.170(3)	0.32(1)	0.30(1)	0.00(1)
	1.1395	1.58(1)	0.16(1)	0.31(1)	0.28(1)	0.04(1)
	1.145	1.56(1)	0.249(2)	0.20(1)	0.24(2)	0.08(2)
	1.15	1.61(1)	0.347(3)	0.11(1)	0.27(1)	0.08(1)
	1.155	1.68(3)	0.45(1)	0.01(1)	0.22(1)	0.16(1)
DP		1.26523	0.15947	0.31368	0.15947	

TABLE II: Estimated spreading exponents for $r = 3.0$ for background values x_i. The deviation from the hyper-scaling relation for $d = 1$ is defined as $\Delta \equiv z_s/2 - (\eta_s + \delta + \theta_s)$. Note that for $b = 0.2$, the natural background state has $x_i \approx 1.235$; for this value, the exponents δ and η_s are close to their DP values. Similarly for $b = -0.2$, the natural background state has $x_i \approx 1.1395$; again δ and η_s are close to their DP values

by the solitons (see Fig. 7b,e). This behavior is distinctly different from what is observed in the various systems belonging to the DP universality class. We have therefore only estimated the spreading exponents for $b = 0.2$ at branch A, and $b = -0.2$ and branch B; in both cases the solitons are not dominant.

Note that the strength of the spreading solitons can be altered by changing the value of the laminar background. By increasing the background to a value above the "natural-initial-state" one, the solitons can be suppressed, while they can be enhanced by a decrease of the laminar value; see Fig. 8.

Our estimates of the dynamical exponents have been done for simulations with a maximum time of 2000 iterations. An active seed is placed in the center of the lattice, surrounded by a laminar background. The seed consists of two active sites, each of which is assigned a random number in the chaotic regime, such that the location is fixed but the values of the active sites differ for each trial in the ensemble. The ensemble size N_s used for statistical averaging and the number of sites in the lattice L have been adjusted to the number of surviving runs the different setups produced, and how far the turbulence propagated out from the seed. A minimum of 200 surviving runs have been used in the averaging.

Our results in table II agree rather well with previously obtained results for probabilistic systems with an infinite number of absorbing states. In particular, the exponents averaged over surviving runs alone definitely seem to be universal as long as the background does not deviate to much from the "natural-initial-state" one. While the values for the sum $\delta + \eta_s$ are very close to the DP value of 0.47315(7), our results for z_s and θ_s deviate from their respective DP values. A very interesting observation is that the hyper-scaling relation is satisfied ($\Delta \simeq 0$) for the majority of different background values. Only for the highest values are significant deviations encountered.

III. STOCHASTIC MODEL.

The propagating structures, which are observed in the CML that we studied in the previous section, appear to play an important role for the transitional behavior. It is, however, numerically very demanding to obtain good statistics for large CMLs and long times. As pointed out already in the introduction, this is the reason why one tries to map such deterministic models to simple stochastic models. Not only may there be more hope to understand such models analytically, they also are much easier to handle from a computational point of view.

In this section we will introduce and study a very simple extension of the Domany-Kinzel cellular automaton which itself is a simple model showing DP behavior. While for the Domany-Kinzel automaton every site can only be active or inactive, we will allow sites to either contain a left or right traveling soliton. As in the CML, these solitons should be generated from active sites only, and we wish to be able to tune their typical lifetime. The only process in which these solitons aid the spreading of activity is by collisions: for simplicity we assume that

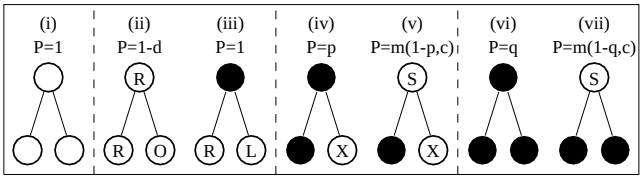


FIG. 9: Schematic definition of our stochastic model. In this picture, the bottom two circles denote possible incoming states, the circle at top denotes the possible stochastic outcome. Our model is defined on a diamond lattice and so one only needs to define the probabilities for certain offspring (active, inactive, right or left traveling soliton) as a function of its two predecessors. Empty circles depict inactive states, black circles are active, "R" and "L" denote right and left-moving solitons, "S" denotes a soliton of arbitrary direction, and "X" finally represents any state (L,R,inactive or active). The notation $m(a,b)$ denotes the minimal value of a and b, and P denotes the conditional probability that this out-coming state occurs. See text for a more elaborate explanation.

with probability *one* a pair of colliding solitons yields a singe active site.

Below we will first discuss the definition of our model in section III A. We will then discuss the mean field equations for our model in section III B, and these will show a transition from second to first order behavior. We will study the statistical properties of our model in section III C. We will illustrate the role of solitons in direct simulations of this model; these simulations will point to the relevance of large "holes" which cannot be "healed" by the solitons. We will discuss the statistical properties of our model near the transition from inactive to active states in the soliton-dominated parameter regime. We will find that the transition is no longer in the DP universality class, since no asymptotic scaling regime can be reached. While the transition shows some characteristics of a first order transition (dependence on initial state for example), the asymptotic situation is not entirely clear: rather we find a regime of long lived transient states between active and inactive regimes.

A. Definition of model

The (1+1) dimensional Domany-Kinzel cellular automaton is defined on a diagonal square lattice where each site can either be active or inactive. The model evolves by parallel updates according to the transition probabilities p and q, corresponding to the probabilities that an empty plus an active site or two active sites respectively produce a single active site. The choice $q = p(2-p)$ corresponds to a realization of directed bond percolation [1].

In our extension the active sites behave like usual directed bond percolation except from the fact that with probability c they can emit a left or right-moving soliton. These solitons have a tunable lifetime and travel ballistically. We assume that the solitons cannot, by themselves, create chaos, except when two solitons collide.

The updating rules are illustrated in figure 9, where the sites can be either inactive (empty), active (black), or contain a left (L) or a right (R) moving soliton (S).
(i) The inactive state: two inactive sites always yield an inactive site. This property ensures that there is a unique absorbing state.
(ii) Soliton propagation: a right moving soliton (R) either dies with probability d, or propagates with probability $(1-d)$ when the "O' state to its right is inactive or another right-moving soliton. The rule for left-moving solitons follows by left-right symmetry.
(iii) Soliton collision: when two oppositely propagating solitons collide, they generate an active site with probability one. This is the only process where solitons lead to spread of active sites. In principle we could generate active sites with a probability less than one, but it may be expected that this does not change the behavior of the model in a qualitative sense.
(iv) Single active sites: a single active site, where X can either be a soliton or inactive site, leads with probability p to a new active site. Note that the spreading of activity is thus not enhanced by individual solitons
(v) Transformation: a single active site can give rise to a soliton (S) with probability $min(1-p,c)$; c denotes the creation rate of solitons. Such a new soliton can be either left or right-moving with equal probability.
(vi) Pair of active sites: two active sites create a new particle with probability q; we restrict ourselves to bond-directed percolation and take $q = p(2-p)$.
(vii) Soliton creation from pair of active states: similar to case (v), a pair of active sites can give rise to solitons with probability $min(1-q,c)$.

B. Mean Field Equations.

To interpret the physical properties of our cellular automaton, a crude insight can be obtained by applying Mean-Field Theory. In this approximation it is reasonable to ignore the differences between left and right traveling solitons, and so our mean field equations are for two concentrations, those of chaotic sites c and solitons s.

b. Equation for Chaotic Sites: Chaotic sites can emit solitons and can be generated by collisions of two solitons; apart from these two rules they behave like DP. Thus, without the solitons the rate equation (without noise) would be $\dot{c} = b_1 c - b_3 c^2$ [13]. To incorporate the creation of an active site when two solitons collide according to rule (iii), the term $b_2 s^2$ needs to be added to this equation. There is no source term linear in s in the rate equation for c, reflecting that we assume that individual solitons do not give rise to activity.

c. Equation for Solitons : There are four processes that influence the solitons. Solitons may decay spontaneously according to rule (ii), and this yields a term $-a_3 s$ in the rate equation for s. Solitons also die upon collision

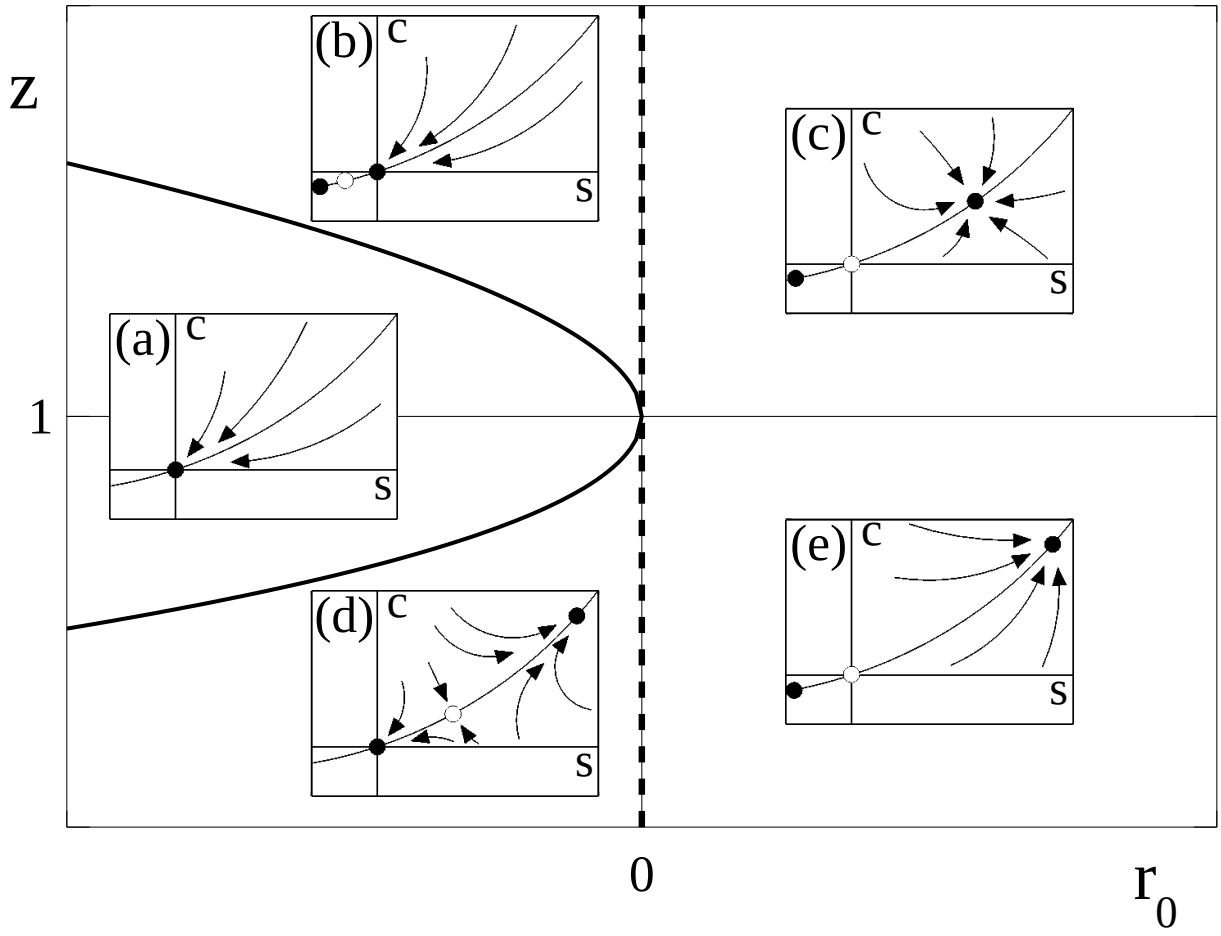


FIG. 10: Dynamical system analysis of the mean field equations (10)-(11). The full and dashed curves show the location in r, z space of the saddle-node and transcritical bifurcations respectively. The five insets (a-e) show schematically the flow in the various regimes of the mean field equations. For more details see text.

leading to a term $\propto -s^2$. Depending on the lifetime of the solitons, either of these two terms may dominate and so we keep both of them; we will see below that this will indeed be a crucial ingredient. Solitons are created from active sites according to rule (v) and (vii). While this in principle yields source terms in the rate equation of s proportional to both c and c^2, we only keep the linear term, since the prefactor for both these terms will be of the same order. Inclusion of the quadratic term does not affect the qualitative dynamics.

The rate equation for the solitons and chaotic sites can then be written as

$$\dot{s} = a_1 c - a_2 s^2 - a_3 s \quad (8)$$
$$\dot{c} = b_1 c + b_2 s^2 - b_3 c^2 \quad (9)$$

where the lifetime of the solitons is set by $1/a_3$ and the spreading rate of the chaotic patches by b_1.

These two equations can be simplified by the introduction of a rescaled of time τ and densities S and C to be

$$\dot{S} = C - S^2 - aS \quad (10)$$
$$\dot{C} = r_0 C + S^2 - uC^2 \quad (11)$$

where

$$a = \frac{a_2 a_3}{a_1 b_2}, \quad r_0 = \tfrac{a_2 b_1}{a_1 b_2}, \quad u = \frac{b_2 b_3}{a_2^2} \quad (12)$$

$$t = \frac{a_2}{a_1 b_2}\tau, \quad s = \tfrac{a_1 b_2}{a_2^2} S, \quad c = \frac{a_1 b_2^2}{a_2^3} C \quad (13)$$

We will now analyze the possible transitions in the mean field Eqs. (12-13).

d. Fixed points The fixed points (S^*, C^*) of the rescaled equations (10)-(11) satisfy $C^* = S^{*2} + aS^*$, where S^* is given by solutions to the fixed point equation

$$Sf(S) = 0 \quad (14)$$
$$f(S) = uS^3 + 2uaS^2 + (ua^2 - 1 - r)S - ar_0 \quad (15)$$

Apart from the trivial fixed point $(S^*, C^*) = (0, 0)$ there may be either 1 or 3 other fixed points which can be found

from solving Eq. (15). It can be shown that Eq. (15) always has one solution for large negative S. This fixed point can be ignored since only points where both S^* and C^* are positive are relevant for our mean field equations (remember that S and C are both concentrations). The two non-trivial fixed points (S_1^*, C_1^*) and (S_2^*, C_2^*) are born in a Saddle-Node bifurcation when the discriminant of Eq. (15) becomes negative. Introducing the parameter $z := a^2 u$ and performing the tedious standard algebra yields that this occurs when

$$z^2 - (2 - 5r_0 - r_0^2/4) + (1 + r_0)^3 = 0 \qquad (16)$$

and so the locus of the saddle-node bifurcation only depends on r_0 and z. It can also be shown that at $r_0 = 0$ always one of the non trivial fixed points crosses through the fixed point of the origin in a transcritical bifurcation. The various types of flows that occur as function of z and r_0 are illustrated in Fig. 10.

As shown in Fig. 10, there are essentially four qualitatively different types of flow and two bifurcations occurring. We will here discuss these flowtypes and their relevance for the dynamics. *(a)* Only the trivial fixed point is present, and is stable. Hence all initial conditions flow to the absorbing state. *(b)* For small soliton lifetime $z > 1$, the two non-trivial fixed points (S_1^*, C_1^*) and (S_2^*, C_2^*) that are born in a saddle-node bifurcation do not lie in the first quadrant and are therefore not relevant for the mean field equations. Hence the situation in *(b)* means that there is a single relevant fixed point at the origin and so the system is in the absorbing state. *(c)* When, for $z > 1$, r_0 crosses through zero from below, (S_1^*, C_1^*) crosses through the origin in a transcritical bifurcation. All initial conditions in the first quadrant flow now to (S_1^*, C_1^*); the mean field equations indicate that there is a finite activity, whose value grows approximately linearly in r_0. The transition at $r_0 = 0$ corresponds to the standard DP transition for $z > 1$. *(d)* For long soliton lifetimes ($z < 1$) the two non-trivial fixed points (S_1^*, C_1^*) (square) and (S_2^*, C_2^*) (triangle) are also created in a saddle-node bifurcation; but in contrast to case (b) both lie in the first quadrant and are therefore *relevant* for the dynamics. Depending on initial conditions, the final state can either be absorbing or active; the incoming manifold of the saddle point acts as a separatrix. The transition that occurs here as the saddle-node bifurcation is crossed leads to a finite jump in the value of c in the active state, which is indicative of a first order transition. *(e)* When, for $z < 1$, r_0 crosses through zero from below, (S_2^*, C_2^*) crosses through the origin in a transcritical bifurcation. All initial conditions in the first quadrant flow now to (S_2^*, C_2^*).

To study the phase transition we shall primarily vary r_0 while keeping a and u fixed. There are three generic choices for z relevant here:

- $z \to \infty$. In this case the solitons have probability 1 to die once they are generated, and so the system is effectively soliton-free. This is the case of pure DP, and the transition takes place at $r_0 = 0$. There is no hysteresis.
- $z > 1$. This is the regime of short soliton lifetimes. Here the solitons do not contribute to any change in the qualitative behavior. An attractive fixed point $S = S_1^* \approx \frac{ar}{z-1}$ emerges for small, positive r_0. This corresponds to $C = C_1^* \approx \frac{a^2 r_0}{z-1}$, such that this fixed point converges towards the DP value $C_1^* \to r_0/u$ for large a. As $r_0 \to 0$ this fixed point converges towards the origin and it changes stability at $r_0 = 0$ (see figure 10), implying that the transition is continuous. Thus, the transition for small soliton lifetimes ($z > 1$) still takes place at $r_0 = 0$ and resembles DP.
- $z < 1$. This the soliton dominated regime where a completely different scenario occurs. For $r_0 > 0$ the behavior is determined by the stable node at $S_2^* \approx a(z^{-1/2} - 1)$. When r_0 becomes negative this fixed point remains stable and away from the origin. Simultaneously the origin becomes attractive and a saddle appears close to the origin at $S = S_1^* \approx \frac{ar_0}{z-1}$. Initial conditions close to the origin will evolve into that point, while initial conditions above the stable manifold for the saddle located at (S_1^*, C_1^*) will converge toward the node (S_2^*, C_2^*). This will go on until the saddle (S_1^*, C_1^*) and the node (S_2^*, C_2^*) merge in a saddle-node bifurcation at $r_0 = r_c(z)$. Below this critical point the origin is globally attractive and every trajectory in the phase space converges towards this. Going back and forth along scenarios (a),(d) and (e) there is hysteresis and so for $z < 1$ we clearly observe a first order transition.

For infinite soliton lifetimes ($a = 0, z = 0$) the critical point is shifted down to $r_0 = -1$. Setting $a = 0$ into equation (15) yields the fixed point $S^* = \sqrt{(1 + r_0)/u}$ which shows that the transition is continuous, but with $\beta = 1/2$ instead of the DP mean-field value, $\beta_{DP} = 1$.

Finally, at the tri-critical point ($z = 1$) equation (15) is reduced to $a^2 f(S) = S^3 + 2aS^2 - a^2 r_0 S - a^3 r_0$. At $r_0 = 0$ the only non-negative root is $S = 0$, but for small positive r_0 a new root appears at $S^* \approx a\sqrt{r_0/2}$. The transition thus remains at $r_0 = 0$ and is continuous, but again with $\beta = 1/2$ instead of the DP value $\beta_{DP} = 1$.

C. Phenomenology and statistical properties of the stochastic model

Let us now discuss the properties of the full stochastic model based on direct numerical simulations. For small but finite values of the soliton lifetime ($d \gg 0$) or for sufficiently small production of solitons ($c \ll 1$) the transition from inactive to active states that occurs when p is increased is of second order and indeed appears to be in the DP universality class. There is, however, also a regime in which the model, at first glance, appears to

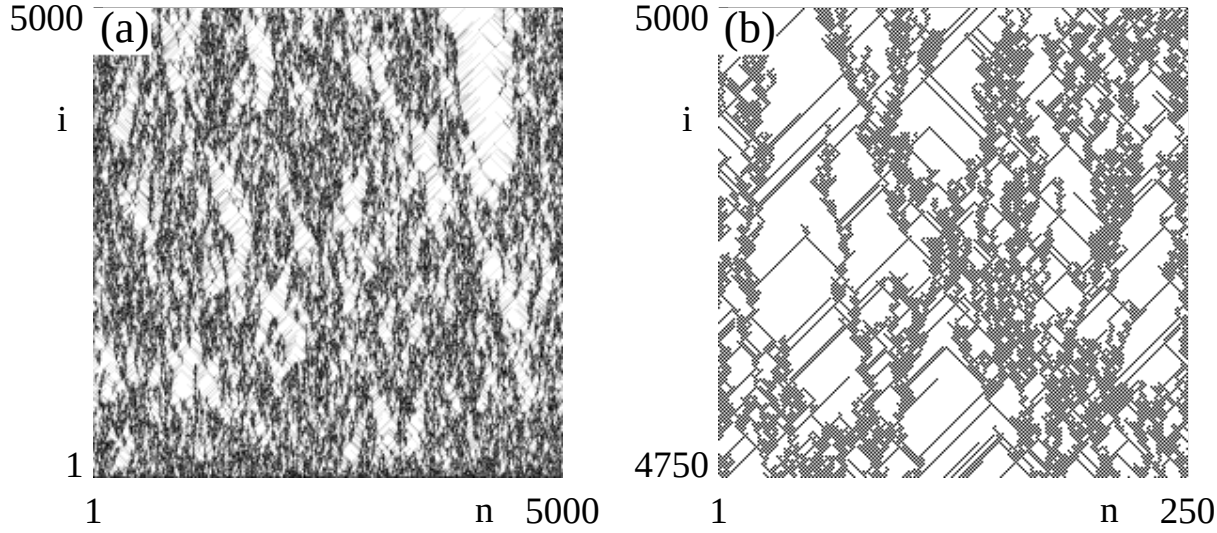


FIG. 11: (a) Large scale dynamics of our stochastic model for $d = 0.01$, $c = 0.1$ and $p = 0.614$. The grey scale corresponds to the number of solitons and active sites coarse grained in a cell of 20 space and 20 time units. (b) Blow up of the dynamics shown in the top left corner of (a).

display a first order transition. In the remainder of the discussion on the stochastic model we will focus on this regime, which shows some interesting new features.

The phenomenology of this regime will be illustrated following Figs. 11-12 where different aspects of the dynamics of our model are shown. The parameters chosen are somewhere in the transitory regime, which in the mean field description corresponds to the regime with two stable fixed points (Fig. 10b).

In Fig. 11a we show the evolution of our model, starting from a fully active state. Fig. 11b is a close-up of the top left corner of Fig. 11a which shows the dynamics of active sites and solitons in detail. At first glance the clusters of activity look extremely similar to the ordinary Domany-Kinzel Cellular Automaton, but after closer inspection it becomes clear that colliding solitons generate new active clusters (one example can be seen in Fig. 11b for $n \approx 50, i \approx 4825$).

While Fig. 11 shows both solitons and active sites, we have shown the coarse grained activity and solitons separately in Figs. 12a-b. Clearly, the soliton density is more uniformly spread, and one can think of the coarse grained dynamics as active clusters surrounded by clouds of solitons.

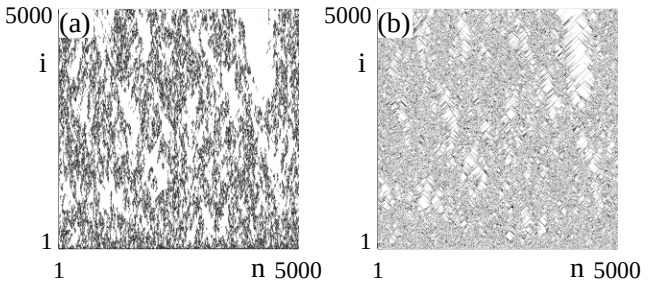


FIG. 12: Concentration of active sites (a) and solitons (b), for the state shown in Fig. 11.

To gain insight in the statistical properties of our model, we have studied the decay of the number of active sites as a function of time, for a range of system sizes L and parameter values p. Here and in the remainder, we keep the soliton-parameters d and c at values 0.01 and 0.1 respectively. In Fig. 13 we show the results of these calculations for p ranging from 0.612 to 0.621.

Clearly, the decay of activity looks quite different from DP. If we focus on the activity as a function of p for a fixed large time τ, we find a very abrupt transition at $p = p_1$ from an inactive to an active state, with a value of the activity given by the "plateau" that can be seen in Fig. 13. This behavior is indicative of a first order transition, consistent with the mean field theory for large soliton lifetimes.

Let us focus on the decay of activity in more detail. When p is small enough, the activity will decay faster than a power-law. When p large enough so that active states will spread, we are certainly above the transition and the activity will reach a plateau value. For DP, there is a critical value where the activity decays as a power-law, but this is not necessarily the case in our model. As shown in Fig. 13 there is a transient decay towards the plateau value which can look like a power-law, as shown in more detail in Fig. 16. For a transient period that in this case goes up to $t \approx 10^3$, it is possible to find values of p such that the decay of m appears to be a power-law with a non-DP exponent. For the example shown, a reasonable scaling can be obtained over 2 decades. We speculate that this may be the origin of the non-universal power-laws observed in coupled map lattices [5, 7]. However, for this to be real asymptotic scaling, one should be

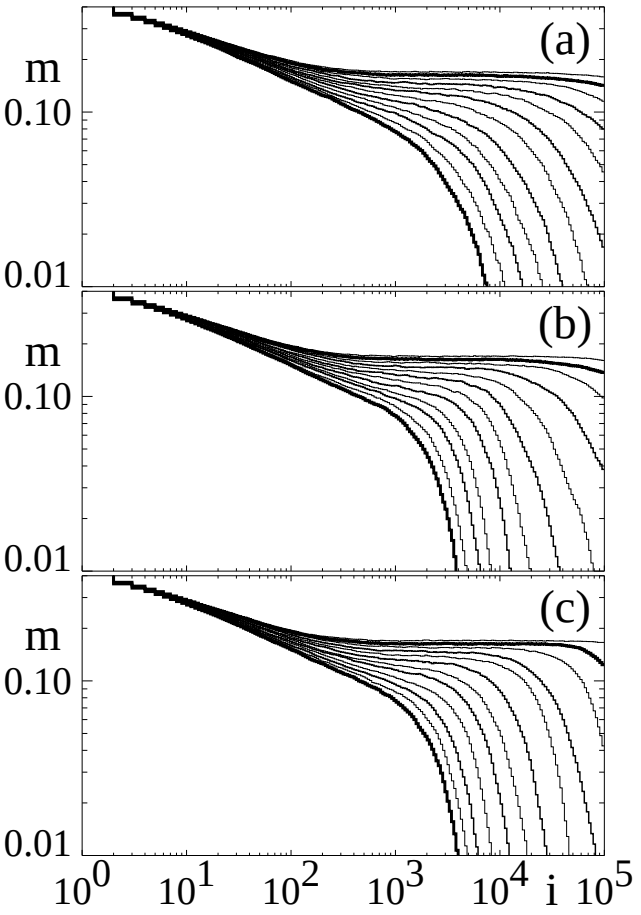


FIG. 13: Decay of average activity m for $c = 0.1$, $d = 0.01$, and $p = 0.610, 0.611, \ldots, 0.621$ (increasing p leads to an increase of activity; the curves with $p = 0.610$ and 0.620 are thicker). Averages are taken over (a) 2000 systems of L=200, (b) 200 systems of L=2000 (c) 20 systems of L=20000.

able to have this scaling extend to arbitrary large times; however the activity curves for sizes 200, 2000 and 20000 all bend downwards at nearly the same time; hence there is no hope that increasing the systemsize extends the time interval over which apparent scaling can be found. For long times the activity either decays rapidly, or first hits a plateau. Clearly, the transition is not an ordinary 2nd order transition.

Is this transition now an ordinary 1st order transition? When we increase the time scale τ where we inspect the average activity, the transition becomes sharper, and the transition value p_1 will shift. We do not see evidence for p_1 going to a well-defined asymptotic value when τ goes to infinity, at least not on the timescales that we can probe numerically, and in this sense the transition is not truly first order.

We will argue now that the plateau indeed does not represent the truly asymptotic behavior. Let us return to Fig. 12, where the activity appears to arrive at the plateau (the overall activity appears to approach a constant). However, around $n \approx 4000, i \approx 3000$ a large

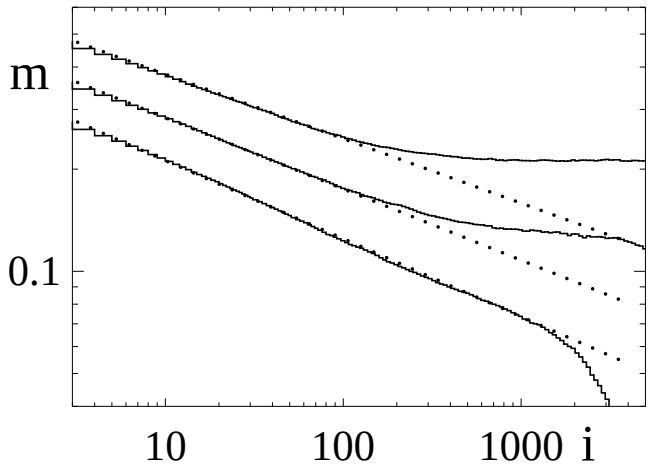


FIG. 14: Average activity m for $c = 0.1$, $d = 0.01$ in an ensemble of 20 systems of $L = 20000$, showing the appearance of quasi-power-law decay. The three curves correspond to $p = 0.612, 0.616$, and $p = 0.62$ respectively, and are shifted by 30% for clarity. The three straight lines corresponds to power-laws with exponents $-0.19, -0.21$ and -0.23. In particular the scaling in the system for $p = 0.612$ looks rather convincing with an exponent of -0.23.

"hole" opens up. Once the size of this hole becomes larger than twice the lifetime of the solitons, it becomes unlikely that colliding solitons will create new activity there and "heal " the hole. In fact, for this particular example the hole did spread out and the system decayed to the inactive state. A closer inspection of the dynamical states that occur when the activity drops below the plateau value, shows that this is the general scenario: the nucleation and subsequent spreading of a large inactive droplet is what dominates the asymptotic decay of the active states here.

The spreading or shrinking of a large hole is governed by the propagation velocity of the coarse grained domain-walls between active and inactive patches. What we have found is that the apparent first order transition point p_1 does not coincide with the point p^* where this velocity changes sign. We illustrate this property by following the dynamics of a large inactive droplet for $p = 0.618$, where

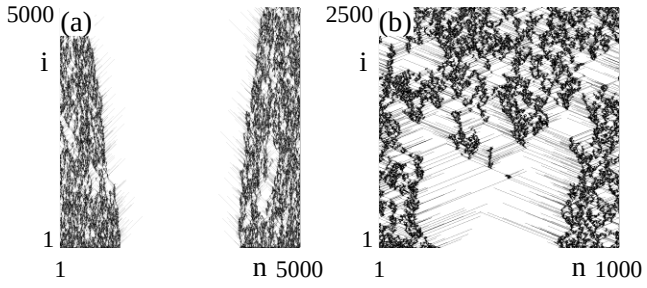


FIG. 15: Dynamics for $c = 0.1, d = 0.01$ and $p = 0.618$, showing that a hole of size 500 is healed (a) while a larger hole of size 2500 is *not* healed (b).

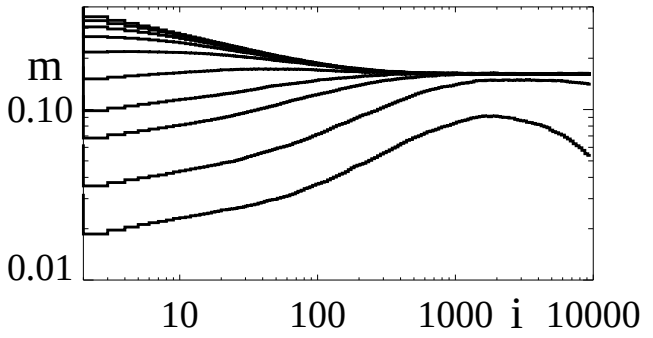


FIG. 16: Evolution of the average activity m in 20 systems of size 20000 for $c = 0.1, d = 0.01$ and $p = 0.621$, i.e., well in plateau regime. Here we vary the initial concentration of active states by randomly distributing active sites through our lattice for $i = 1$. These activities are, respectively, $1.0, 0.85, 0.7, 0.55, 0.4, 0.25, 0.15, 0.1, 0.05$ and 0.025. For the latter two cases, the plateau is not reached, even though initially the activity is increasing. That the long time behavior ($i > 200$) depends on the initial concentration is reminiscent of a first order transition.

the system has a well defined plateau in the activity (see Fig. 13). Thus $p > p_1$, but nevertheless, a hole of size 5000 grows as can be seen in Fig. 15. A hole of size 500 is healed for these same parameter values, as shown in Fig. 15.

The solitons in our model thus introduce an additional length-scale of order $1/d$, and as a result the size of the *inactive* holes becomes of importance. When such holes are smaller than $2/d$, solitons will penetrate deeply enough to collide and create new patches of activity within this hole. Since the first order transition is triggered by the solitons, this indicates that the velocity of the domain wall is not strongly dependent on these degrees of freedom. This is in accord to the results from the mean field analysis, if we assume that the properties of the domain walls are still governed by the trivial fixed point with $C = 0$.

The difference between the spreading of a small active cluster and the behavior of an homogeneously active state indicates that the initial concentration of active sites plays a role. This is illustrated in Fig. 16 where we follow the evolution of the activity for a range of initial concentrations of activity for $p = 0.621$. For initial activities in the range from 1 to 0.1, the same plateau value is reached, but for initial activities of 0.05 and smaller, there is an initial increase of the activity after which the activity rapidly decays; the plateau is never reached.

In Fig. 17 we show the evolution of the activity m divided by the number of surviving clusters for the same parameter values. For small systems these plots are very different from the ones averaged over all systems (Fig. 13); in the present case there is a typical activity in each system which rapidly disappears. We interpret this as further evidence that the nucleation of large holes dominates the eventual decay. For larger systems this

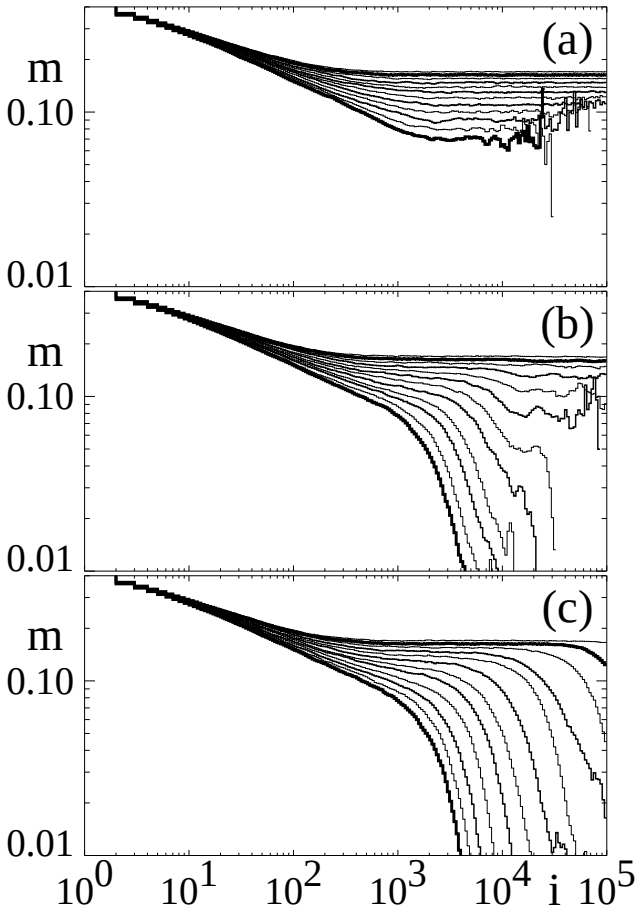


FIG. 17: Average activity divided by the number of active systems, for the same parameter values as shown in Fig. 13.

effect disappears because the time it takes for a hole to engulf the whole system is large.

IV. DISCUSSION

The overall picture that emerges from our study is that the transition to spatio-temporal intermittency is strongly influenced by coherent ballistically traveling "solitons", which, even though they have a finite life-time, change the nature of the transition and can introduce first order like behavior. That such a scenario is relevant is supported by recent evidence for a discontinuous transition to spatio-temporal chaos in the damped Kuramoto-Sivashinsky equation [23], which is well-known to support localized ballistically moving excitations, or "pulses" [24].

We build our conclusions upon an extension, using two dimensional local maps, of the Chaté-Manneville coupled map lattice. We thereby gain an additional parameter, which turns out to tune the importance and life-time of the solitons. For this coupled map lattice we find, depending on parameters, evidence for both continuous phase transitions in the universality class of Directed Per-

colation with infinitely many absorbing states and for first order behavior.

To understand this behavior, we have developed a stochastic model generalizing the Domany-Kinzel cellular automaton. In this model, the active sites can emit solitons and by colliding, the solitons can create new active sites. Simulations of this model, together with the appropriate mean field theory, support the existence of both continuous and discontinuous transitions. With the stochastic model one can look at the behavior on much larger length and time scales. One thereby discovers that the active states close above the discontinuous transitions are actually metastable, and will finally decay when a sufficiently large droplet nucleates. Such breakdown of first order behavior has been predicted by Hinrichsen [25]. We have not been able to pin down exactly how the nucleation time and eventual decay depends on system size, but it is not ruled out that the truly asymptotic behavior is still given by Directed Percolation in accordance with the predictions of Hinrichsen.

Even though the first order behavior is probably not truly asymptotic, it appears very clearly over a surprisingly long range of intermediate time scales, and would thus be relevant in the interpretation of experiments. We further show that this feature can lead to long power like transients displaying non-universal "critical exponents," and we believe that such transients are the origin of the observed non-universality in the transition to spatio-temporal intermittency.

[1] E. Domany and W. Kinzel, *Phys. Rev. Lett.*, **53**, 311 (1984).

[2] T. Bohr, M. H. Jensen, G. Paladin and A. Vulpani, *Dynamical Systems Approach to Turbulence* (Cambridge University Press 1998).

[3] H. Chaté, Nonlinearity **7**, 185 (1994); M. van Hecke, Phys. Rev. Lett. **80**, 1896 (1998).

[4] P. Grassberger and T. Schreiber, *Physica D*, **50**, 177 (1991).

[5] H. Chaté and P. Manneville, *Physica D*, **32**, (1988), 409.

[6] T. Bohr, M. van Hecke, R. Mikkelsen and M. Ipsen, Phys. Rev. Lett. **86**, 5482 (2001).

[7] H. Chaté and P. Manneville, *Phys. Rev. Lett.*, **58**, 112 (1987).

[8] H. Chaté in *Spontaneous Formation of Space-Time Structures and Criticality*, ed. by T. Riste and D. Sherrington, 273 (Kluwer 1991).

[9] S. Ciliberto and P. Bigazzi, *Phys. Rev. Lett.*, **60**, 286 (1988); F. Daviaud, M. Dubois and P. Bergé, *Europhys. Lett.*, **9**, 441 (1989); M. Rabaud, S. Michalland and Y. Couder, *Phys. Rev. Lett.*, **64**, 184 (1990); S. Michalland and M. Rabaud, Physica D, **61**, 197 (1992).

[10] A. Novick-Cohen and G. I. Sivashinsky, Physica D, **20**, 237 (1986).

[11] Y. Pomeau, *Physica D*, **23**, 3 (1986).

[12] G. Grinstein and M. A. Muñoz in *Fourth Granada Lectures in Computational Physics* ed. by P. Garrido and J. Marro, *Lecture Notes in Physics*, **493**, 223 (Springer, Berlin 1997).

[13] H. Hinrichsen, Adv. in Phys. **49**, 815 (2000).

[14] P. Grassberger, *Z. Phys. B*, **47**, 365 (1982).

[15] H. K. Janssen, *Z. Phys. B*, **42**, 151 (1981).

[16] J. Rolf, T. Bohr and M. H. Jensen, *Phys. Rev. E* **57**, R2503 (1998)

[17] M. Henon, *Comm. Math. Phys.* **50**, 69 (1976).

[18] J. M. Houlrik, I. Webman and M. H. Jensen, *Phys. Rev. A* **41**, 4210 (1990); J. M. Houlrik and M. H. Jensen, in *Theory and applications of coupled maps lattices*, (ed. K. Kaneko, John Wiley and Sons Ltd., 1993).

[19] M. A. Muñoz, R. Dickman, A. Vespigniani and S. Zapperi, *Phys. Rev. E*, **59**, R6175 (1999).

[20] P. Grassberger and A. de la Torre *Ann. Phys. (N.Y.)* **122**, 373 (1979).

[21] J. F. F. Mendes, R. Dickman, M. Henckel and M. C. Marques, *J. Phys. A* **27**, 3019 (1994).

[22] M. A. Munoz, G. Grinstein and Y. Tu, Phys. Rev. E **56**, 5101 (1997); M. A. Munoz, G. Grinstein and R. Dickman, J. Stat. Phys. **91**, 541 (1998).

[23] K. R. Elder, J. D. Gunton and N. Goldenfeld, Phys. Rev. E, **56**, 1631 (1997); M. Paniconi and K. R. Elder, Phys. Rev. E **56**, 2713 (1997).

[24] N. J. Balmforth, Ann. Rev. Fluid Mech. **27**, 335 (1995).

[25] H. Hinrichsen, cond-mat 0006212 (2000).